Photoemission simulation for photocathode design: theory and application to copper and silver surfaces.

B. Camino[1], T.C.Q. Noakes[2], M. Surman[2], E.A. Seddon[2] and N. M. Harrison[1]

[1]*Department of Chemistry, Imperial College London, South Kensington, London, SW7 2AZ, UK*

[2]*Daresbury Laboratory, Daresbury, Warrington, WA4 4AD, UK* *

(Dated: January 27, 2016)

Abstract

Fourth generation light sources, also called free electron lasers (FELs) are particle accelerators which use relativistic free electrons as a lasing medium. They are able to generate photons ranging the whole electromagnetic spectrum from infrared to X-rays. As opposed to 3rd generation light sources, such as synchrotrons, in FELs electrons undergo a single pass through the machine. There is, therefore, no way to improve the electron beam by focussing and beam shaping within a storage ring. This means that, obtaining a bright and low emittance electron beam directly from the photocathode is mandatory in order to design high performance FELs. To achieve this goal a clear understanding of how the emission process is influenced by structure, morphology and composition of the photocathode's surface is needed. This is difficult from an experimental point of view because often the atomic scale details of the surface whose emission has been measured are unknown. A predictive theoretical approach capable of determining the effects of surface structure on emission is therefore or great interest. A model to extend the well known three step model (as proposed by Berglund and Spicer) to surface calculations is discussed in this paper. It is based on a layer-by-layer decomposition of the surface electronic structure that can be calculated through reliable and efficient DFT calculations. The advantage of this approach with respect to other existing photoemission calculations is being able to correlate directly the photoemission to the electronic, atomic and chemical structure of the surface. The proposed approach retains, therefore, the simple chemical intuition in the study of surface modifications and their effect on the photoemission. The approach is validated in calculations of the emission from clean copper and silver surfaces. The ability of the model to simulate the change in photoemission in response to adsorbates is tested by simulating monolayers of oxygen, hydrogen and lithium on the copper (111) surface.

PACS numbers:

*Electronic address: nicholas.harrison@imperial.ac.uk

Contents

I. INTRODUCTION

Free electron lasers (FELs) are the state of the art in terms of light generation for time resolved spectroscopy [1, 2]. In these devices, the lasing medium are free electrons, which are emitted from a photocathode, accelerated by a linear accelerator and pass through an undulator to generate an intense photon beam. FELs give access to a broad wavelength range (THz to X-Rays) and provide pulses of radiation of the order of the fs, in the time scale and six order of magnitude brigther than the previous sources [3–5]. Such short pulses of radiation allow the probing of the ultra-small (such as single molecule diffraction [5, 6]) and of the ultra-fast (structural and electron dynamics [7]). The applications of the FELs radiation are many and varied covering different branches of the science such as biological structural studies (eliminating the need to crystallize the proteins/viruses [5, 6]) and materials studies.

One of the main differences with respect to previous generation light sources is that FELs are single pass machines: electrons pass throught the accelerator one time only introducing a dependance of the quality of the emitted radiation on the initial electron beam properties [8]. The quality of the emitted radiation (in terms of brightness and response time) depends on the quality of the electrons beam used to generate it. Therefore, photocathodes are a key component to modern accelerator systems and a broad international research programme [9] is now aimed at their improvement. An empirical approach has provided materials for the above mentioned applications; however, their efficiency is limited and a clear understanding of the emission mechanism hinders the rational design of new photocathodes.

Typically PE calculations are based either on just the bulk electronic structure or simplified models of the surface [10–12]. In order to achieve a rational design of new emitting materials it is necessary to understand how the surface structures influences the photoemission process. In this paper, a simple approach to compute photoemission from surfaces is presented. Firstly, density functional theory (DFT) calculations are performed on surface models. Modern DFT methods facilitates calculations on rather realistic models of surface environments that take into account their chemistry, morphology and structure. In order to connect the DFT surface electronic structure to the measured photoemission an extension of the well known three-step-model [13] to surface calculations is reported. A projection of the wave function onto pseudo atomic orbitals is used in order to calculate a layer-by-layer

decomposition of the surface electronic structure. This approach is expected to reproduce satisfactorily the emission process while retaining the chemical intuition needed to understand the effect of morphology, composition and structure.

The above described method was tested on model systems, copper and silver clean surfaces as often used as emitting materials in photocathodes. Oxygen, hydrogen and lithium monolayers were simulated as additives on the copper (111) surface. These species were chosen in order to simulate the effect of atoms characterised by higher and lower electronegativity with respect to the copper substrate. Their effect on the band structure, work function and quantum efficiency spectrum is calculated and discussed.

In section II details of the method are outlined. Photoemission simulations on copper and silver surfaces are reported in section III as a test case.

II. COMPUTATIONAL DETAILS

Electronic exchange and correlation were computed in the generalised gradient approximaition (GGA) to density functional theory (DFT) using the PBE functional [14] and a plane wave (PW) basis set as implemented in CASTEP [15]. The variation in the total electronic energy per atom of the order of 10^{-5} eV was found for a plane wave energy cutoff of 500 eV and a Monkhorst-Pack [16] sampling of the Brillouin zone (BZ) of the bulk primitive cell of 14x14x14. Tolerance on the geometry optimisation is set to be lower than 10^{-5} eV/atom and a Gaussian smearing of 0.05 eV was used. Copper has an fcc structure (space group 225) whose optimised lattice paramenter is 3.63 Å (experimental lattice parameter is 3.60 Å [17]). These parameters were used for all the calculations reported here. The accuracy of the copper bulk band structure was compared to GW calculations [18] and good agreement was found.

Surfaces are simulated using a thin slab model which has two-dimensional periodicity in the xy plane and is of finite thickness in the z direction. The slab is modelled in a 3D periodic cell with a vacuum space separating adiacent slabs. The surface formation energy was computed as a function of the vacuum gap spacing and the thickness of the slab. Variations of less than 10^{-3} J/m^2 were achieved for a vacuum height of 15 Å and a thickness of six layers on. The ten layer slabs are used to simulate clean surfaces. In order to simulate the interaction of adsorbates with the surface slabs consisting of six layers of

copper are used. Two external atoms (one on each side of the slab) make the total thickness eight layer. The main features (surface states and work function value) are described within a difference of 8x10^{-3} eV between the ten and six layer slab. This makes the latter adequate for the study of changes in the quantum efficiency (QE) due to surface modifications.

Photoemission from the surface is sensitive to the formation of surface states. These states also play an important role in surface reactivity. The identification of surface states is facilitated by comparison of the band structure of a slab model with the surface projected band structure. A description of the tecnique used to obtain the projected band structure can be found in [19]. The bulk electronic states are defined within the first BZ of the bulk crystal as $\epsilon_i(\mathbf{k}) \equiv \epsilon_i(\mathbf{k}_{||}, \mathbf{k}_\perp)$ where $\mathbf{k}_{||} \equiv (\mathbf{k_x}, \mathbf{k_y})$ and $\mathbf{k}_\perp \equiv (\mathbf{k_z})$. The electronic states of the 2D periodic slab are defined within the first BZ of the surface unit cell as $\epsilon_i(\mathbf{k}_{||})$, where $\mathbf{k} \equiv (\mathbf{k_x}, \mathbf{k_y}, \mathbf{0})$. In the calculation of the surface projected band structure the same path chosen for the slab is used in the bulk calculation. This is achieved by creating a rotated bulk cell with two vectors in the surface plane in order to define suitable $\mathbf{k}_\perp$, which is sampled at different values and the different $\bar{\epsilon_i}(\mathbf{k}_{||}, \mathbf{k}_\perp)$ are reported at $\mathbf{k}_{||}$. An example of surface projected band structure of copper (111) and (100) surfaces in the region around Γ is reported in [20].

For a particular approximation of the surface electronic structure, the quantum efficiency is calculated here according to Eq. 1:

$$Q.E.(\omega, l) = \frac{\sum_{i=1}^{VBM} \sum_{f=WF}^{\infty} \int_{BZ} |\mathbf{M}_{i,f}^{\mathbf{k}}|^2 \; \delta(E(\omega) - (\epsilon_f^{\mathbf{k}} - \epsilon_i^{\mathbf{k}})) \mathbf{W}_{i,l}^{\mathbf{k}} \; \mathbf{I}_l(\omega) \; \mathbf{esc}_{i,l}^{\mathbf{k}} \; \mathbf{H}(\mathbf{p}_\perp > 0) \frac{d\mathbf{k}}{(2\pi)^3}}{\sum_{i=1}^{VBM} \sum_{f=VBM+1}^{\infty} \int_{BZ} |\mathbf{M}_{i,f}^{\mathbf{k}}|^2 \; \delta(E(\omega) - (\epsilon_f^{\mathbf{k}} - \epsilon_i^{\mathbf{k}})) \; \mathbf{W}_{i,l}^{\mathbf{k}} \; \mathbf{I}_l(\omega) \frac{d\mathbf{k}}{(2\pi)^3}} \tag{1}$$

This is an extension of Spicer's three step model [13] to surface simulations. The QE is defined through the energy of the incident photon (ω) and the layer (l) from which the electron is emitted. The QE is measured in units of electrons / photon but, Eq. 1 gives a unitless result because it calculates the ratio between photons leading to emission with respect to the total number of photons reaching the surface. For the sake of simplicity, in the following, QE is reported as unitless. The integral is performed over the $\mathbf{k}$ points of the surface first BZ. In the denominator the summation involves all initial (i) and final states (f), whereas in the numerator only the final states leading to emission of the excited electron, *i.e.* the states above the vacuum level (WF), are included. $\mathbf{M}_{i,f}^{\mathbf{k}}$ is an optical

matrix element accounting for the coupling of the valence band i and the conduction band f at $\mathbf{k}$. Its square is the probability for the transition to occur between the two states:

$$\mathbf{M}^{\mathbf{k}}_{i,f} =< \psi^{f}_{\mathbf{k}} | \mathbf{u} \cdot \mathbf{r} | \psi^{i}_{\mathbf{k}} > \tag{2}$$

In Eq. 2, $\mathbf{u}$ defines the polarization of electric field of the incident light and $\mathbf{r}$ is the momentum operator. $[\delta(E(\omega) - (\epsilon^{\mathbf{k}}_{f} - \epsilon^{\mathbf{k}}_{i})i)]$ is a delta function ensuring the energy conservation in the process: only states whose energy difference matches the energy of the photon are included in the summation. $\mathbf{W}^{\mathbf{k}}_{i,l}$ is the proportion (weight) of the density of states (DOS) attributed to layer l as estimated by projection of the DOS onto atomic orbitals (AO). The AO used here were those used in the construction of the PP. The projection is used to measure the contribution of each layer to the initial state and is central to the layer-by-layer decomposition of the emission central to the application of Eq. 1. The efficacy of this approach for identifying the contribution of adsorbate induced surface states is demonstrated below. $\mathbf{I}_{l}(\omega)$ represent the intensity of light incident on the "l-th" layer and $\mathbf{esc}^{\mathbf{k}}_{i,l}$ is the escape function for the electron excited from initial state i in $\mathbf{k}$ characterised by $\mathbf{W}^{\mathbf{k}}_{i,l}$. The escape function is estimated here using the universal mean free path, where the electron-electron scattering is the only phenomenon preventing electron emission [21]. This curve is determined by one parameter, the inelstic mean free path (IMFP) length which can be considered constant in the range of energy studied here. It was chosen to be 5.54 Å for copper and 6.13 Å for silver. These values are calculated as the average of those reported in the literature [22–26]. The heaviside step function $\mathbf{H}(\mathbf{p}_{\perp} > 0)$ ensures that only final state electrons characterised by a positive momentum along the direction perpendicular to the surface ($\mathbf{p}_{\perp}$) contribute to the QE. Since the momentum parallel to the surface ($\mathbf{p}_{\parallel}$) is conserved during the transition, $\mathbf{p}_{\perp}$ varies according to the energy of the final state j. $\mathbf{p}_{\perp}$ is determined by the conservation of energy such that:

$$E_{f} = \epsilon^{\mathbf{k}}_{f} - E_{v} = \frac{1}{2m}(\mathbf{p^{2}_{x}} + \mathbf{p^{2}_{y}} + \mathbf{p^{2}_{z}}) = \frac{\hbar}{2m}(\mathbf{k^{2}_{x}} + \mathbf{k^{2}_{y}} + \mathbf{k^{2}_{z}}) \tag{3}$$

$$\mathbf{p_{z}} = \mathbf{p}_{\perp} = (E_{f} - \frac{\hbar^{2}}{2m}(\mathbf{k^{2}_{x}} + \mathbf{k^{2}_{y}}))^{\frac{1}{2}} \tag{4}$$

Where the final energy E_f is equal to the energy of the final state above the vacuum energy ($\epsilon^{\mathbf{k}}_{f} - E_{v}$). If the z component is negative the electron is absorbed within the crystal

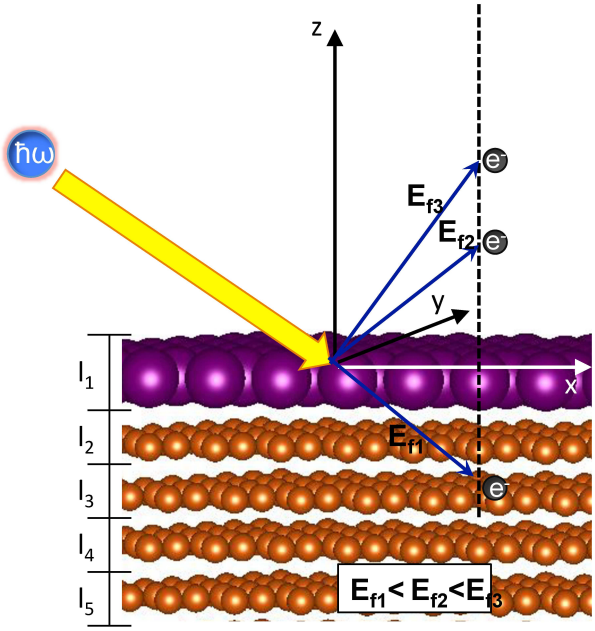

FIG. 1: Schematic representation of the effect of the conservation of the momentum parallel to the surface during the electron emission.

and does not contribute to the quantum efficiency. This highlights an important feature of photoemmission which is that the the lower the final energy of the excited electron (*i.e.* the photon energy), the higher is the contribution to the QE from $\mathbf{k}$ points close to Γ because electrons with larger values of $\mathbf{k}$ will not be emitted but absorbed by the substrate. The effect of this restriction on the electron momentum is schematically shown in Fig. 1, where electrons excited from the same $\mathbf{k}$ point (same $\mathbf{k_x}$ and $\mathbf{k_y}$) at three different photon energies is represented. E_{f1} is notionally sufficient energy to overcome the work function, but its $\mathbf{p}_\perp$ component, calculated according to Eq. 4 is negative. This means that upon excitation, the electron is travelling inside the surface. E_{f2} provides a positive $\mathbf{p}_\perp$, which means the electron is emitted from the surface. The higher the E_f becomes, the closer to the z axis the electron is travelling (compare E_{f3} and E_{f2} in Fig. 1).

III. RESULTS AND DISCUSSION

Prior to computing the surface electronic structure of the surface, the atomic structure of the slab model is determined by energy minimisation. The computed surface energies of the three low index surfaces of copper and silver are reported in Table I. The values obtained are somewhat lower than the those reported previously in the literature which were calculated

at local density (LDA) or generalized gradient approximation (GGA) levels of theory using local basis sets [27] or linear muffin-tin orbitals in the atomic-sphere approximation (ASA) [28, 29]. This is to be expected as the variational freedom of the PW basis set used in the current study provides a more accurate description of the spread of electron density into the vacuum region which is, by necessity, constrained within the ASA or with standard local basis sets [30]. The surface energy of silver is in agreement with other PW calculations [31] (maximum deviations of 8 %). As an additional test, a calculation using the Quantum Espresso code with the same exchange-correlation functional, **k** sampling grid and plane wave energy cutoff as the CASTEP calculations was performed. It yields an almost identical surface energy (differences lower than 5 x 10^{-3} mJ/m^2). Larger variations are seen when the pseudopotential is altered, for example, using the projector augmented wave (PAW) method produces a variation of 6% in the surface energy relative to using the PBE pseudopotential. Despite these numerical discrepancies in the absolute surface energy, which are inherent in the pseudopotential approach, the relative surface energies of different facets are more consistently described. For copper the (110) and (100) surfaces energies are 17% and 16% higher than the (111) one, respectively. Similar results are obtaiend for silver, where the (110) and (100) surfaces energies are 16% and 9% higher than that of (111), respectively.

The equilibrium crystallite morphology can be estimated using the Wulff construction [32, 33]. From the morphology an estimate of the surface area of each facet present in a polycrystalline sample can be calculated. The Wulff construction of a copper crystallyte is displayed in Fig. 2. The shape of this construction is in agreement with transmission electron microscopy (TEM) images of copper nanoparticles synthesized at low H_2 pressure [34]. Hydrogen is used as reducing agent and is present at a pressure of 1.5 mbar while TEM images were recorded. The shape of such nanoparticles changes dramatically in presence of oxidising or reducing agents. However, at low H_2 pressure it is expected to be comparable to simulations performed in vacuum. For both materials, the major contribution to the surface area is due to the lowest energy (111) surface, representing 69% of the copper and 63% of the surface area of silver crystallites (see Table I for details). Since the (111) surface is the most stable for the two metals studied here and therefore likely to be predominant in polycrystalline sample it is used below as the basis for our calculations of the variations in QE induced by surface adsorbates.

The work function of the surfaces reported in Table I was calculated as the difference

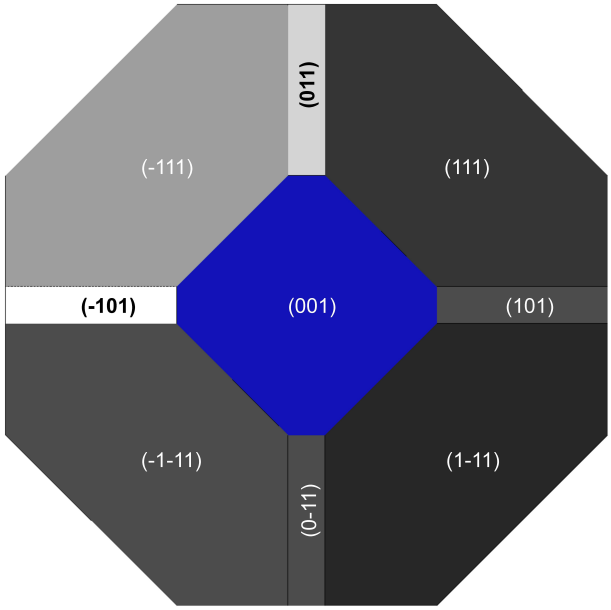

FIG. 2: A Wulff construction of the equilibrium morphology for a Cu crystal.

between the Fermi energy and the average of the potential between neighbouring slabs [35]. For both copper and silver the (111) surface exhibits the highest work function, 4.50 eV and 4.25 eV, respectively. The surface having the lowest work function among the ones studied here is the Ag (110) surface, whose work function is 3.53 eV. The effect of such a low values (compared to the other surfaces) on the photoemission is discussed below. In order to compare the calculated work function values to data obtained on polycrystalline samples, the average work function was calculated as an average over a crystallite by weighting the surface energy of each facet with its fractional contribution to the total surface area. The resulting work functions are 4.41 eV for copper and 4.13 eV for silver which is in reasonable agreement with values reported in literature for such metals: 4.4-5.3 eV and 4.2-4.7 eV for copper and silver samples, respectively calculated using linear-muffin-tin-orbitals Green's-function theory [29]. From photoemission experiments work function values between 4.3 eV and 5.1 eV for copper and between 4.2 eV and 4.7 eV for silver have been deduced [36–38].

In Fig. 3 the surface and bulk projected band structures for the low index surfaces of Cu and Ag are displayed. The energy levels whose contribution from a surface layer is higher than 15% ($\mathbf{W}^{\mathbf{k}}_{i,l} > 15\%$, where l is the top layer, see Section II), are identified as surface states and depicted in red. By comparing the surface band structure to the corresponding bulk projected one it is possible to determine that these states are not present in the latter confirming they are introduced by the surface. These band structures are in

overall good agreement with respect to those deduced from measurements of the surface electronic structure [39–47]. For example, the very well known state in the L gap of the copper (111) surface band structure is calculated to have an energy minimum at 0.45 eV below the Fermi level and crossing it at 0.28 Å^{-1} along the Γ to M direction in reciprocal space. This compares very well to the most recent values deduced from angle resolved photoemission experiments (ARPES) and confirmed by KKR band structure calculations [42], where the minimum energy is 0.37 eV and crossing of the Fermi level at 0.2 Å^{-1} along the Γ to M direction. The other surface state on the Cu (111) surface is near the K symmetry point. In this work this state is found at 2.7 eV which is comparable to the 3.0 eV found in ARPES experiments [43].

The comparisons made above suggest that the current PW-PP calculations using the GGA exchange-correlation functional are able to reproduce the measured work function, position of the surface states to the accuracy of $\pm$ 0.3 eV with respect to previous calculations and experimental data. It is, therefore, reasonable to expect that this description of the surface electronic structure can be used to calculate the trends in QE according to Eq. 1 reliably.

One advantage of the method adopted here is that it lends itself to a decomposition of the total QE into contributions from each layer. The total quantum efficiency corresponding to the sum of the contribution coming from every layer is represented by the thick black line in the plots in Fig. 5. Within this model, more than half of the QE is due to emission from the top-most atomic layer of the surface. The contribution from the second atomic layer is 11.4 % and 11.7 % for copper and silver (111) surfaces, respectively and it becomes negligible starting from the fifth layer (less than 4 % for both metals).

The principal factor in determining the photoemission threshold is the work function of the surface. It is important, however, to recognise that the first emitted electrons do not correpond to a photon energy equal to the work function. Two other factors determine the photoemission threshold (see Eq. 1): the energy conservation during the transition, $\delta(E(\omega) - (\epsilon_f^{\mathbf{k}} - \epsilon_i^{\mathbf{k}}))$, and the constraint on the momentum perpendicular to the surface $\mathbf{p}_\perp$ (see Eq. 3 and 4). Taking the Cu (111) surface as an example, the first significative photoemission (QE $> 10^{-5}$) is observed for a photon energy of 4.90 eV, despite the fact that its computed WF is 4.50 eV. This is because the lowest energy difference between states in the valence and conduction band is 4.90 eV. In Table I the QE at a photon energy of 5.5 eV

is reported. This photon energy was chosen in the wavelength range of the optical lasers used in photocathode applications. Furthermore, it facilitates a comparison of the QE of different facets that is representative of the whole spectrum. The QE from a polycrystalline sample computed as a facet weighted average was found to be 4.6 x 10^{-4} for copper and 6.5 x 10^{-4} for silver. These computed values are primarily intended to reveal trends in variations of QE with surface modification. They are, nevertheless, in general agreement with measurements of the absolute QE made on these metals. These range between 10^{-6} and 10^{-3} measured for polished and mirror like samples in vacuum [36]. This is in reasonably agreement with the quantum efficiency simulated in this work.

In order to examine the effects of surface bond formation and charge transfer between the metal and adsorbed species three model systems were considered. The adsorption of monolayers of O, H or Li on the copper (111) surface was modelled. The first two species were selected because they are well know contaminants of photocathode's surfaces. The third one is representative of the effect of alkali metals, which are often used in order to enhance the cathode's QE The three adsorbates are representative of atoms characterised by higher or lower electronegativity with respect to copper and exhibit different effects on the work function and surface band structure, which will be discussed. The model used in this study allows to disentangle the effects of these changes on the QE. Furthermore, O and H are very well know contaminants on photocathode surfaces. Li is modelled to study the effect of alkali metals since they are used as coating agent in order to increase the quantum efficiency of photocathodes [48]. The adsortion of these three species on the copper (111) surface has been extensively discussed in the literature [49–51]. The fcc and hcp sites are found to be the most stable, with differences in their adsorption energy of the order of 10^{-2} eV/atom between the two sites, for the three types of atoms. The geometry used in this study is the one where the external atom occupies an hcp three fold hollow site on the surface. The spacing among atoms in the monolayer is the same as the lattice parameter of the slab cell (2.57 Å). The adsorption energy is -0.62 eV/atom for oxygen, -0.24 eV/atom for hydrogen and -0.12 eV/atom for lithium with respect to the energy of $^1/_2$ O_2, $^1/_2$ H_2 and bulk Li. In Fig. 6 the structure and surface state band structure for each model are reported. The blue bands correpond to the states where the contribution of the external atom is higher than 15%.

In the oxygen covered copper (111) surface the major effect is the change in WF, where

an increase of 3.56 eV is observed (see Table II). This is caused by the charge transfer of 0.42 eV, according to a Mulliken population analysis, between the copper topmost atom of the surface and the oxygen monolayer. This generates a surface dipole that stabilises the electronic states of the surface relative to vacuum. Some additional surface states are also introduced in the band structure (blue bands in Fig. 6). They are particularly apparent at the Γ and at M high symmetry points, just above and below the Fermi level, respectively. The former does not affect the quantum efficiency being in the conduction band, but below the vacuum level. The latter will enhance the surface photoemission providing the surface with more states at the top of the valence band from where electrons can be emitted. The WF determines the lowest photon energy able to cause photoemission. No photoemission is, therefore, predicted to happen at energy lower than 8.53 eV.

The hydrogen monolayer has a minor influence on the WF, decreasing it by only 0.06 eV. If this were the only effect the photoemission should start at lower photon energy with respect to the clean surface. Instead the edge of photoemission is found to be 0.1 eV higher with respect to the clean surface. This rather curious behaviour is due to changes in the surface band structure. Indeed, hydrogen does not introduce additional surface state that contribute to photoemission and shifts the two surface states closer to the Fermi level at Γ in the clean surface (compare top right panel in Fig. 3 to central right panel in Fig. 6) to the bottom of the conduction band. In this case the two effects mean that the quantum efficiency is 30% lower than the clean surface at a photon energy of 5.5 eV.

For the lithium monolayer the WF is lowered by 0.78 eV and surface states in the valence band near Γ are introduced (see Fig. 6). This lowers the edge of photoemission of 0.7 eV and enhances the quantum efficiency at 5.5 eV of 37% with respect to the clean surface.

IV. CONCLUSIONS

A method to simulate photoemission from surfaces is presented. It is based on a layer-by-layer decomposition of the electronic structure of the surface. This can be calculated from first principles using reliable and accurate density functional theory calculations. In modern implementations such calculations can be applied to the morphology, composition and structure of complex and realistic representations of material surfaces. The photoemission is computed from the electronic structure in a simple extension of the three step model.

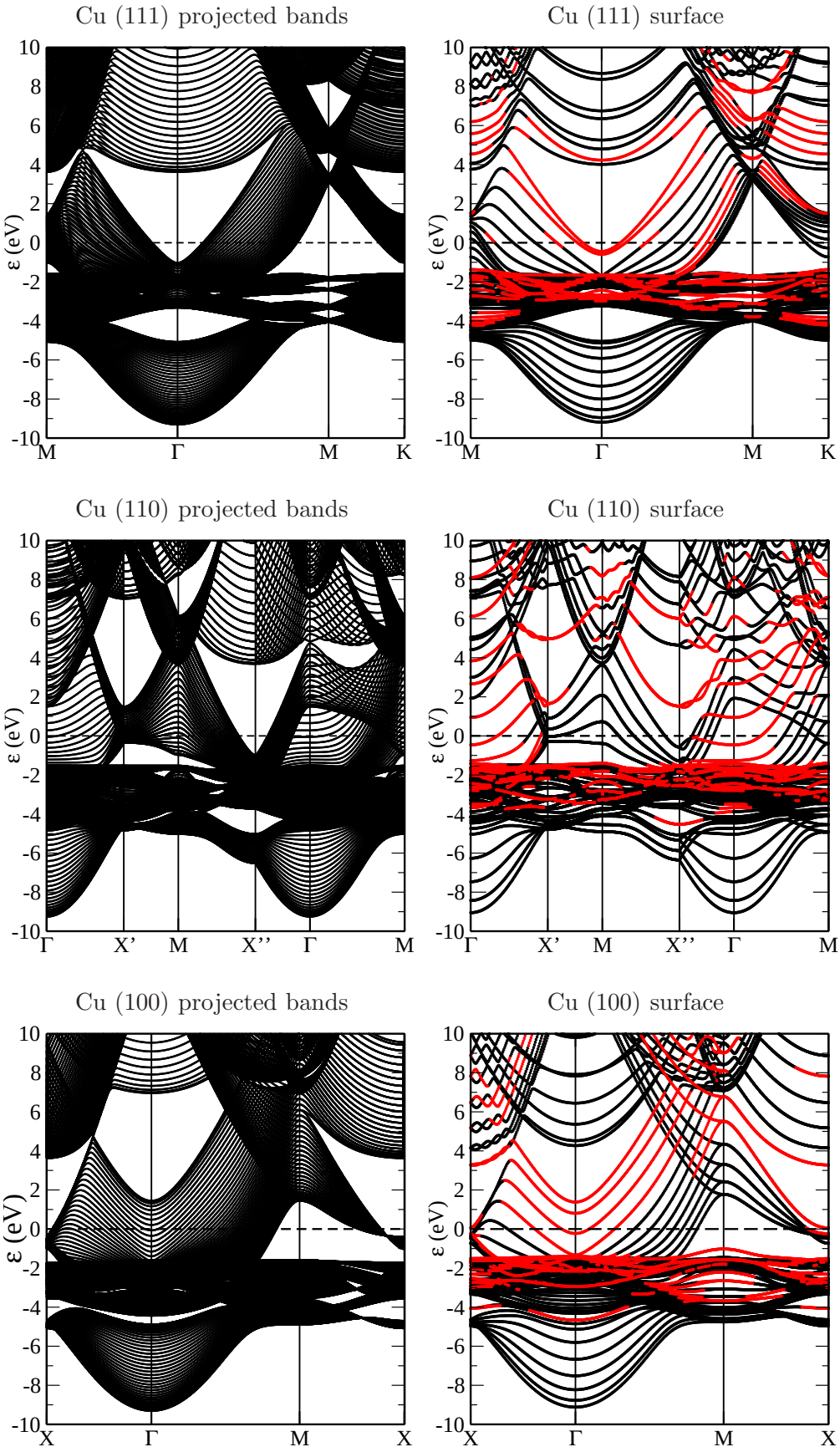

FIG. 3: Copper (111), (110) and (100) surfaces. Left: pojected band structure. Right: surface band structure. Surface states, identified according to the procedure described in Section II are depicted in red. States equally delocalised on the whole slab are shown in black.

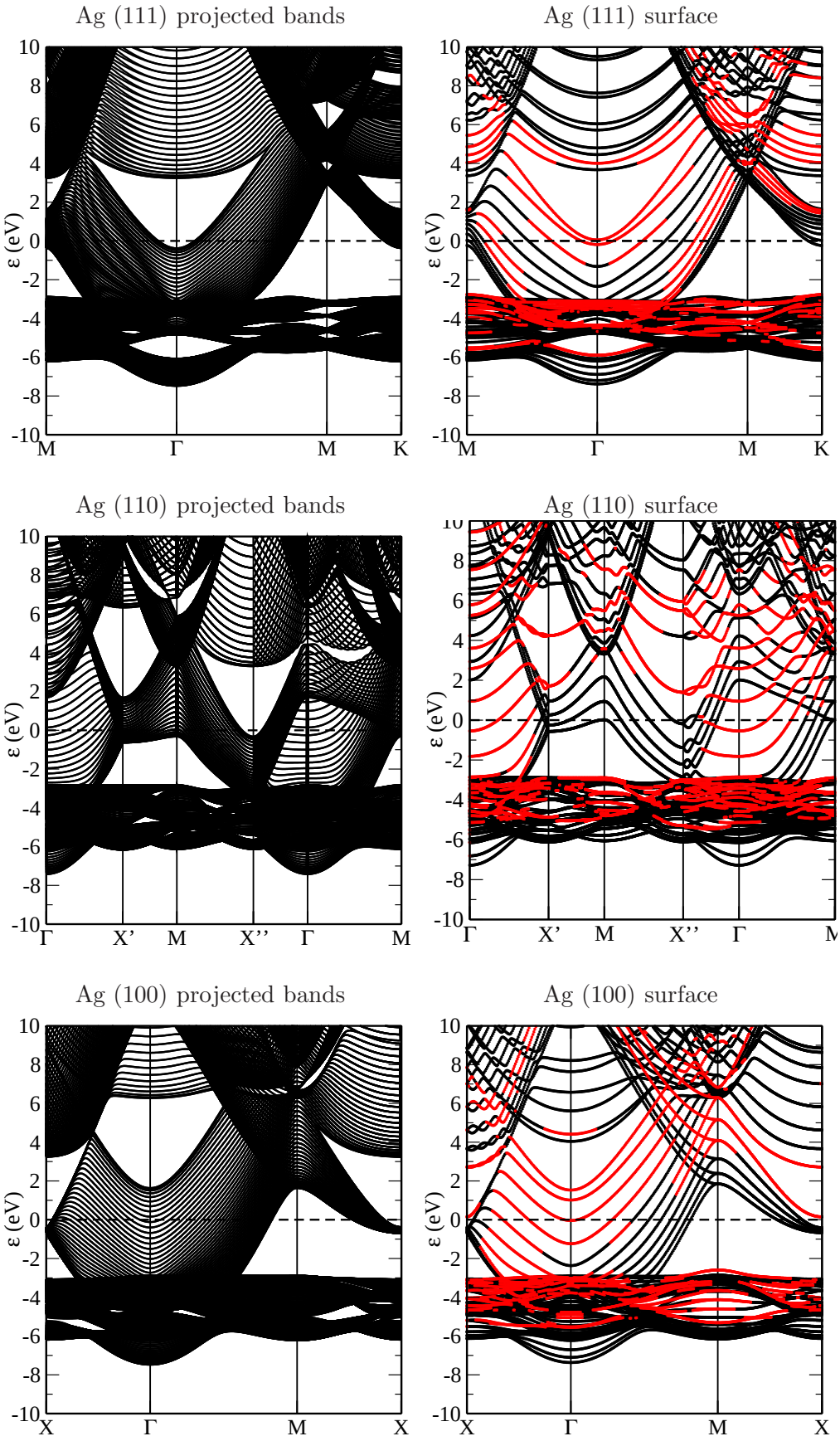

FIG. 4: Silver (111), (110) and (100) surfaces. Left: pojected band structure. Right: surface band structure. Surface states, identified according to the procedure described in Section II are depicted in red. States equally delocalised on the whole slab are shown in black.

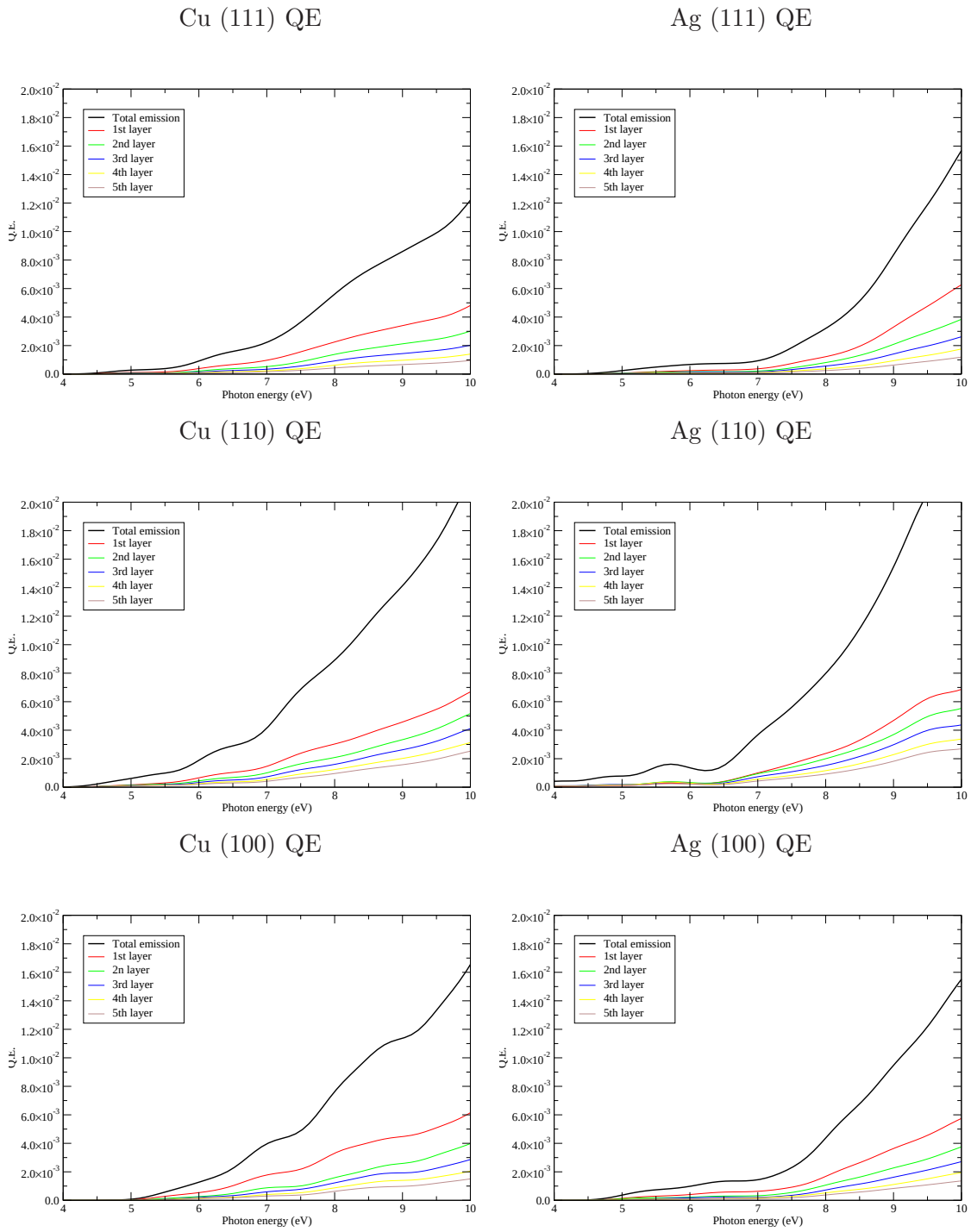

FIG. 5: Calculated QE as a function of the photon energy for the three copper and silver surfaces. The energy axis is shown between 4 and 10 eV and the QE axis between 0 and 2 x 10^{-2}. This setup is mantained for all QE plots reported here in order to provide an easier comparison among different graphs.

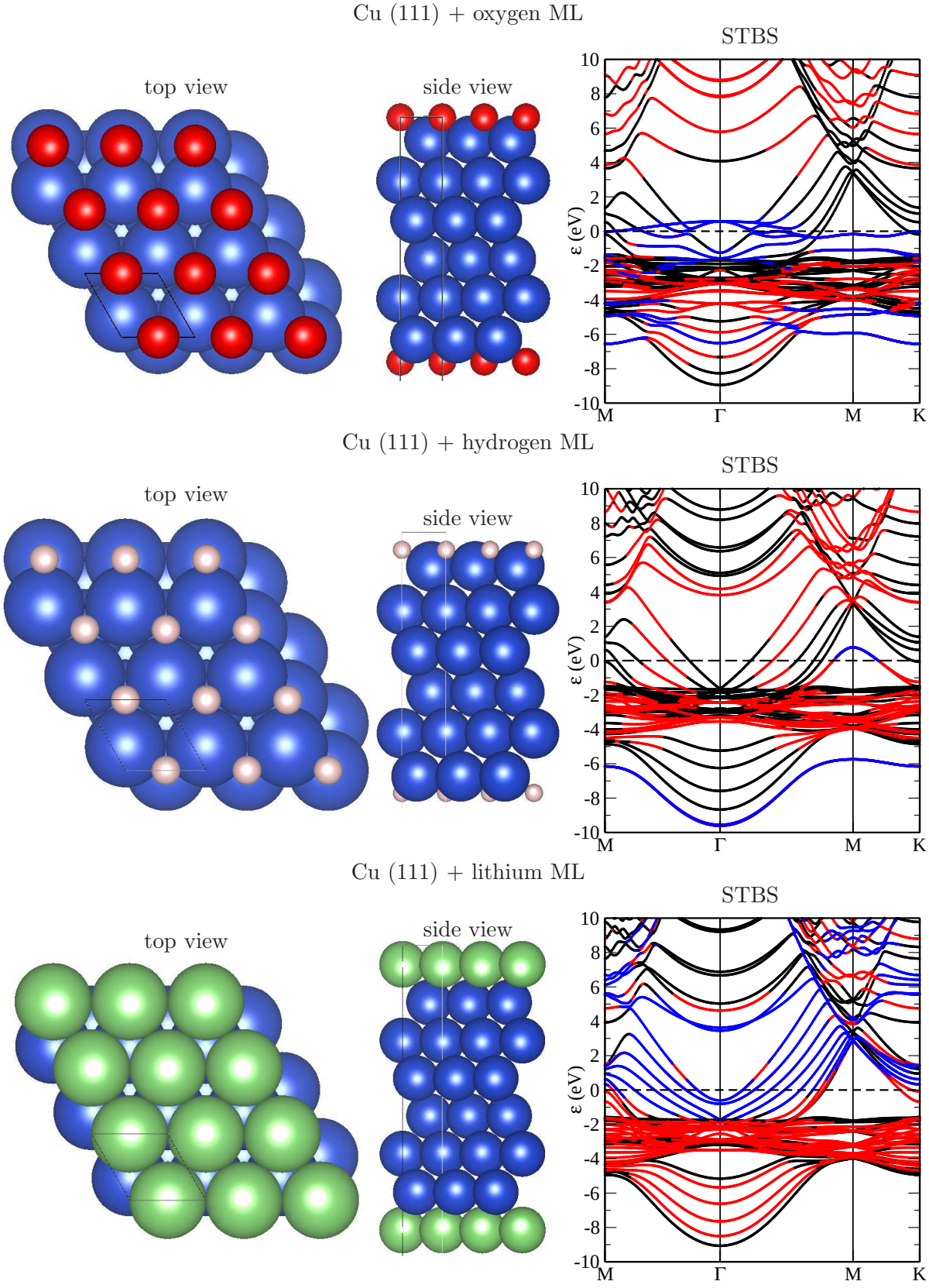

FIG. 6: Cu (111) surface interacting with oxygen, hydrogen and lithium. Left: geometry of the optimised structure. Right: surface band structure. The oxygen/hydrogen/lithium and the first copper layer states are depicted in blue and red, respectively. States equally delocalised on the whole slab are shown in black.

	Cu			Ag		
	(111)	(110)	(100)	(111)	(110)	(100)
$\mathbf{E_{surf}}$ eV/atom	0.47	0.90	0.63	0.38	0.71	0.48
J/m^2	1.32	1.55	1.53	0.80	0.93	0.88
WF (eV)	4.50	4.13	4.27	4.25	3.53	4.10
QE ($\hbar\omega = 5.5eV$)	3.5 x 10^{-4}	9.8 x 10^{-4}	6.1 10^{-4}	5.4 x 10^{-4}	1.2 x 10^{-3}	7.1 x 10^{-4}
%**Wulff**	69.1 %	9.10 %	21.8 %	62.9 %	9.84 %	27.3 %

TABLE I: Surface energy, work function quantum efficiency at photon energy of 5.5 eV and % of each surface according to a Wulff construction for the Cu and Ag (111), (110) and (100) surfaces.

	WF (eV)	QE (eV) ($\hbar\omega = 5.5eV$)
Clean	4.50	7.3 x 10^{-4}
Oxygen	8.06	0.00
Hydrogen	4.44	4.8 10^{-4}
Lithium	3.72	1.0 x 10^{-3}

TABLE II: Work function and quantum efficiency for the Cu (111) surface when atomically clean and interacting with oxygen, hydrogen and lithium.

This approach is validated in calculations of the photoemission from the clean surfaces of two well know emitting materials: copper and silver. It is then used to predict the changes induced by typical surface modifications by examining the effect of Adsorbing oxygen, hydrogen and lithium monolayers to the copper (111) surface. These adsorbates were chosen to illustrate the combined effects of surface bonding and charge transfer into, and out of, the metal surface. It is found that oxygen adsorption increases the work function by more than 3 eV and does not introduce surface states that are effective for photoemmision. Hydrogen adsorption has minimal impact on the computed emission, whereas lithium decreases the work function and the emission at a typical wavelength for photocathode operation ($\hbar\omega$= 5.5 eV) is predicted to be enhanced by 37% relative to the clean surface. The approach presented provides a flexible and robust computational tool for examining the variations in photoemision induced by chemical modifications to surfaces and will be used in future work

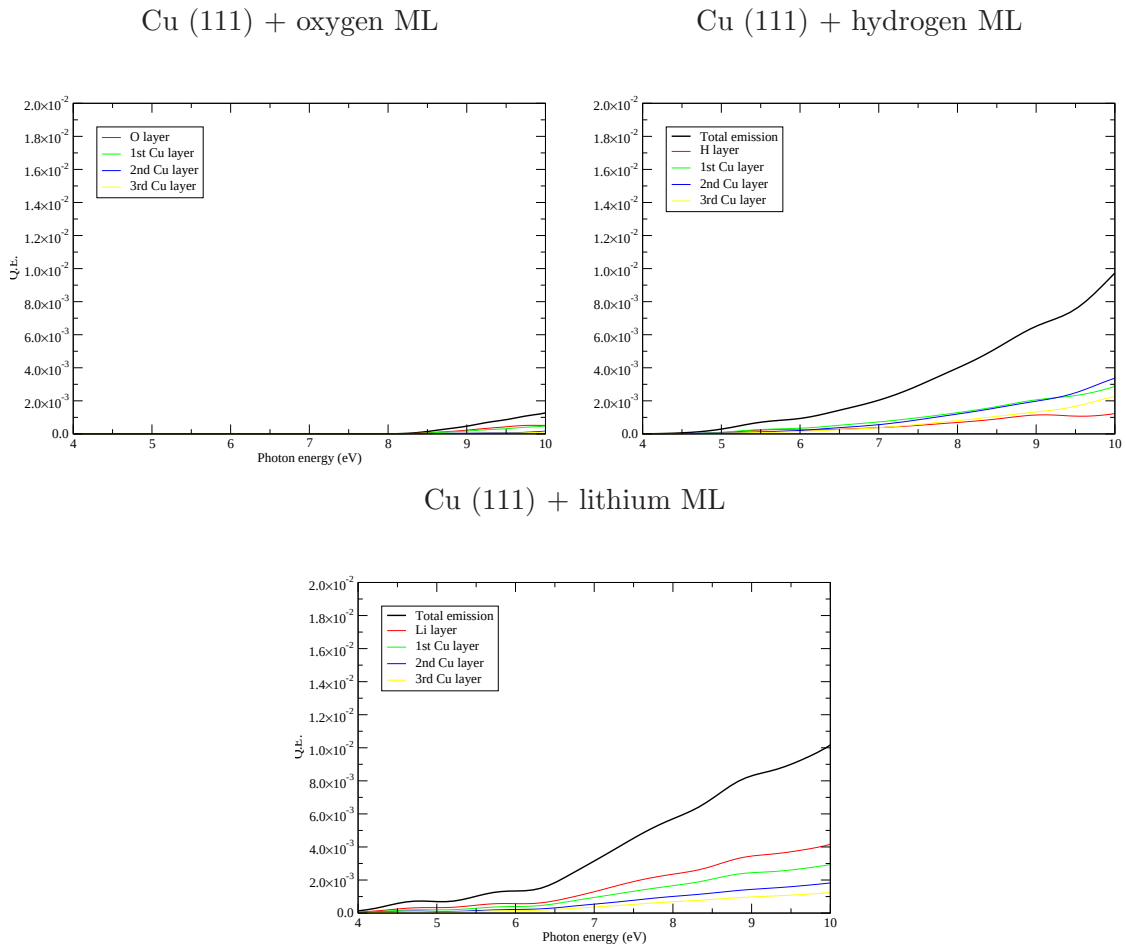

FIG. 7: Calculated QE as a function of the photon energy for the (111) copper surfaces when interacting with a monolayer of oxygen, hydrogen and lithium.

to assist in the design new photocathode materials.

Acknowledgments

Via our membership of the UK's HEC Materials Chemistry Consortium, which is funded by EPSRC (EP/L000202), this work used the ARCHER UK National Supercomputing Service (http://www.archer.ac.uk). The project is carried out in collaboration with the ASTeC group based at the Daresbury Laboratories and it is founded by the Science and Technology Facilities Council.

---

[1] J. M. J. Madey, Journal of Applied Physics **42** (1971).

[2] Z. Huang and K.-J. Kim, Phys. Rev. ST Accel. Beams **10**, 034801 (2007), URL http://link.aps.org/doi/10.1103/PhysRevSTAB.10.034801.

[3] M. Chergui, Faraday Discuss. **171**, 11 (2014), URL http://dx.doi.org/10.1039/C4FD00157E.

[4] W. R. Flavell, F. M. Quinn, J. A. Clarke, E. A. Seddon, N. R. Thompson, M. A. Bowler, M. D. Roper, S. L. Smith, H. L. Owen, B. D. Muratori, et al., *4gls: the uk's fourth generation light source* (2005), URL http://dx.doi.org/10.1117/12.632523.

[5] J. Hajdu, Current Opinion in Structural Biology **10**, 569 (2000), ISSN 0959-440X, URL http://www.sciencedirect.com/science/article/pii/S0959440X00001330.

[6] G. Huldt, A. Szke, and J. Hajdu, Journal of Structural Biology **144**, 219 (2003), ISSN 1047-8477, analytical Methods and Software Tools for Macromolecular Microscopy, URL http://www.sciencedirect.com/science/article/pii/S1047847703001825.

[7] J. C. H. Spence, Faraday Discuss. **171**, 429 (2014), URL http://dx.doi.org/10.1039/C4FD00025K.

[8] D. Dowell, I. Bazarov, B. Dunham, K. Harkay, C. Hernandez-Garcia, R. Legg, H. Padmore, T. Rao, J. Smedley, and W. Wan, Nuclear Instruments and Methods in Physics Research Section A: Accelerators, Spectrometers, Detectors and Associated Equipment **622**, 685 (2010), ISSN 0168-9002, URL http://www.sciencedirect.com/science/article/pii/S0168900210006868.

[9] B. W. J. McNeil and N. R. Thompson, Nat Photon **4**, 814 (2010).

[10] M. Lueders, A. Ernst, W. M. Temmerman, Z. Szotek, and P. J. Durham, Journal of Physics: Condensed Matter **13**, 8587 (2001), URL http://stacks.iop.org/0953-8984/13/i=38/a=305.

[11] W. Schattke, Progress in Surface Science **54**, 211 (1997), ISSN 0079-6816, URL http://www.sciencedirect.com/science/article/pii/S0079681697000051.

[12] J. Minr, J. Braun, S. Mankovsky, and H. Ebert, Journal of Electron Spectroscopy and Related Phenomena **184**, 91 (2011), ISSN 0368-2048, advances in Vacuum Ultraviolet and X-ray PhysicsThe 37th International Conference on Vacuum Ultraviolet and X-ray Physics (VUVX2010), URL http://www.sciencedirect.com/science/article/pii/S0368204811000156.

[13] C. N. Berglund and W. E. Spicer, Phys. Rev. **136**, A1030 (1964), URL http://link.aps.

org/doi/10.1103/PhysRev.136.A1030.

[14] J. P. Perdew, K. Burke, and M. Ernzerhof, Phys. Rev. Lett. **77**, 3865 (1996), URL http://link.aps.org/doi/10.1103/PhysRevLett.77.3865.

[15] S. J. Clark, M. D. Segall, C. J. Pickard, P. J. Hasnip, M. J. Probert, K. Refson, and M. Payne, Z. Kristall. **220**, 567 (2005).

[16] H. J. Monkhorst and J. D. Pack, Phys. Rev. B **13**, 5188 (1976), URL http://link.aps.org/doi/10.1103/PhysRevB.13.5188.

[17] D. P. Woodruff, D. L. Seymour, C. F. McConville, C. E. Riley, M. D. Crapper, N. P. Prince, and R. G. Jones, Phys. Rev. Lett. **58**, 1460 (1987), URL http://link.aps.org/doi/10.1103/PhysRevLett.58.1460.

[18] A. Marini, R. Del Sole, A. Rubio, and G. Onida, Phys. Rev. B **66**, 161104 (2002), URL http://link.aps.org/doi/10.1103/PhysRevB.66.161104.

[19] C. Pisani, *Lecture notes in chemistry: quantum-mechanical ab-initio calculation of the properties of crystalline materials* (1996).

[20] S. Vijayalakshmi, A. Fhlisch, F. Hennies, A. Pietzsch, M. Nagasono, W. Wurth, A. Borisov, and J. Gauyacq, Chemical Physics Letters **427**, 91 (2006), ISSN 0009-2614, URL http://www.sciencedirect.com/science/article/pii/S0009261406009183.

[21] C. Powell, Journal of Electron Spectroscopy and Related Phenomena **47**, 197 (1988), ISSN 0368-2048, URL http://www.sciencedirect.com/science/article/pii/0368204888850126.

[22] C. J. Powell and A. Jablonski, Journal of Physical and Chemical Reference Data **28** (1999).

[23] A. P. Sorini, J. J. Kas, J. J. Rehr, M. P. Prange, and Z. H. Levine, Phys. Rev. B **74**, 165111 (2006), URL http://link.aps.org/doi/10.1103/PhysRevB.74.165111.

[24] W. S. M. Werner, Surface and Interface Analysis **31**, 141 (2001), ISSN 1096-9918, URL http://dx.doi.org/10.1002/sia.973.

[25] J. D. Bourke and C. T. Chantler, Phys. Rev. Lett. **104**, 206601 (2010), URL http://link.aps.org/doi/10.1103/PhysRevLett.104.206601.

[26] I. Nagy and P. M. Echenique, Phys. Rev. B **85**, 115131 (2012), URL http://link.aps.org/doi/10.1103/PhysRevB.85.115131.

[27] K. Doll and N. Harrison, Chemical Physics Letters **317**, 282 (2000), ISSN 0009-2614, URL http://www.sciencedirect.com/science/article/pii/S0009261499013627.

[28] L. Vitos, A. Ruban, H. Skriver, and J. Kollr, Surface Science **411**, 186 (1998), ISSN 0039-6028, URL http://www.sciencedirect.com/science/article/pii/S003960289800363X.

[29] H. L. Skriver and N. M. Rosengaard, Phys. Rev. B **46**, 7157 (1992), URL http://link.aps.org/doi/10.1103/PhysRevB.46.7157.

[30] F. F. Sanches, G. Mallia, and N. M. Harrison, **1494**, 339 (2013), URL http://journals.cambridge.org/article_S1946427413002364.

[31] A. Chatterjee, S. Niwa, and F. Mizukami, Journal of Molecular Graphics and Modelling **23**, 447 (2005), ISSN 1093-3263, URL http://www.sciencedirect.com/science/article/pii/S1093326305000057.

[32] G. Wulff, Z. Kristallogr. **34**, 449 (1901).

[33] C. Herring, Phys. Rev. **82**, 87 (1951), URL http://link.aps.org/doi/10.1103/PhysRev.82.87.

[34] P. L. Hansen, J. B. Wagner, S. Helveg, J. R. Rostrup-Nielsen, B. S. Clausen, and H. Topse, Science **295**, 2053 (2002), http://www.sciencemag.org/content/295/5562/2053.full.pdf, URL http://www.sciencemag.org/content/295/5562/2053.abstract.

[35] C. J. Fall, N. Binggeli, and A. Baldereschi, Journal of Physics: Condensed Matter **11**, 2689 (1999), URL http://stacks.iop.org/0953-8984/11/i=13/a=006.

[36] F. Pimpec, C. Milne, C. Hauri, and F. Ardana-Lamas, Applied Physics A **112**, 647 (2013), ISSN 0947-8396, URL http://dx.doi.org/10.1007/s00339-013-7600-z.

[37] T. SrinivasanRao, J. Fischer, and T. Tsang, Journal of Applied Physics **69** (1991).

[38] H. B. Michaelson, Journal of Applied Physics **48** (1977).

[39] F. Reinert, G. Nicolay, S. Schmidt, D. Ehm, and S. Hüfner, Phys. Rev. B **63**, 115415 (2001), URL http://link.aps.org/doi/10.1103/PhysRevB.63.115415.

[40] N. V. Smith, Phys. Rev. B **32**, 3549 (1985), URL http://link.aps.org/doi/10.1103/PhysRevB.32.3549.

[41] N. Smith, Applications of Surface Science **2223, Part 1**, 349 (1985), ISSN 0378-5963, URL http://www.sciencedirect.com/science/article/pii/0378596385900674.

[42] A. A. Ünal, C. Tusche, S. Ouazi, S. Wedekind, C.-T. Chiang, A. Winkelmann, D. Sander, J. Henk, and J. Kirschner, Phys. Rev. B **84**, 073107 (2011), URL http://link.aps.org/doi/10.1103/PhysRevB.84.073107.

[43] Y. Yang, S. C. Wu, F. Q. Liu, K. Ibrahim, H. J. Qian, S. H. Lu, and F. Jona, Phys. Rev. B

54, 5092 (1996), URL http://link.aps.org/doi/10.1103/PhysRevB.54.5092.

[44] M. Hengsberger, F. Baumberger, H. J. Neff, T. Greber, and J. Osterwalder, Phys. Rev. B **77**, 085425 (2008), URL http://link.aps.org/doi/10.1103/PhysRevB.77.085425.

[45] R. Courths, B. Cord, H. Wern, and S. Hfner, Physica Scripta **1983**, 144 (1983), URL http://stacks.iop.org/1402-4896/1983/i=T4/a=031.

[46] A. Winkelmann, C. Tusche, A. A. nal, M. Ellguth, J. Henk, and J. Kirschner, New Journal of Physics **14**, 043009 (2012), URL http://stacks.iop.org/1367-2630/14/i=4/a=043009.

[47] F. Baumberger, T. Greber, and J. Osterwalder, Phys. Rev. B **64**, 195411 (2001), URL http://link.aps.org/doi/10.1103/PhysRevB.64.195411.

[48] L. Kong, A. G. Joly, T. C. Droubay, Y. Gong, and W. P. Hess, Applied Physics Letters **104**, 171106 (2014), URL http://scitation.aip.org/content/aip/journal/apl/104/17/10.1063/1.4874339.

[49] L. Padilla-Campos, A. Toro-Labb, and J. Maruani, Surface Science **385**, 24 (1997), ISSN 0039-6028, URL http://www.sciencedirect.com/science/article/pii/S0039602897000897.

[50] J. Strmquist, L. Bengtsson, M. Persson, and B. Hammer, Surface Science **397**, 382 (1998), ISSN 0039-6028, URL http://www.sciencedirect.com/science/article/pii/S0039602897007590.

[51] Y. Xu and M. Mavrikakis, Surface Science **494**, 131 (2001), ISSN 0039-6028, URL http://www.sciencedirect.com/science/article/pii/S0039602801014649.